Cognitive Radar Signal Processing

Antonio De Maio
Università degli Studi di Napoli "Federico II"
Dipartimento di Ingegneria Elettrica e delle Tecnologie dell'Informazione
Via Claudio 21, I-80125 Napoli, Italy
ademaio@unina.it

Alfonso Farina
Technical Consultant
previous with Selex ES (now retired) Rome, Italy
alfonso.farina@outlook.it

ABSTRACT

Cognitive radar is a new paradigm to conceive the next radar generation characterized by unique and amazing features inspired to mental abilities and processes related to knowledge. Introduced by Haykin [1] and Guerci [2], it is attracting huge attention within the radar community during the last few years. The key concept is that radar system performance can be enhanced through a continuous and coordinated feedback between the transmitter and receiver which implies a dynamic adaptation of the sensor's algorithms to the operational context and environmental replies. This paper discusses the biological inspiring principles of cognitive radar and analyzes the resulting conceptual architecture. Then, three challenging radar signal processing applications, which can significantly benefit from cognition, are illustrated highlighting the potential performance benefits achievable with the awesome pro-active paradigm.

1. Cognitive Radar Paradigm

Cognitive dynamic systems have been inspired by the unique neural computational capability of brain and the viewpoint that cognition (in particular the human one) is a form of computation. Some exemplifications within this new class, which is undoubtly among the hallmarks of the 21st century, are cognitive radar, control, radio, and some other engineering dynamic architectures. S. Haykin published two pioneering articles in the context of the cognitive radar [3], [4]. The key idea behind this new paradigm is to mimic the human brain as well as that of other mammals with echolocation capabilities (bats, dolphins, whales, etc). They continuously learn and react to the stimulations from the surrounding environment according to four basic processes: perception-action cycle, memory, attention, and intelligence. This last observation highlights the importance of specifying which are the "equivalents" of the aforementioned activities in a cognitive radar. This is thoroughly discussed in [2], [5], and [6].

The perception-action process, schematized as in Figure 1, has the fundamental task of sounding the environment. Radar transmitter through the waveform emission stimulates the background with the goal to obtain a response (i.e. a radar echo) from it. The mentioned response is perceived by the radar receiver which plays the equivalent role of the human senses.

(a) General.   (b) Radar.
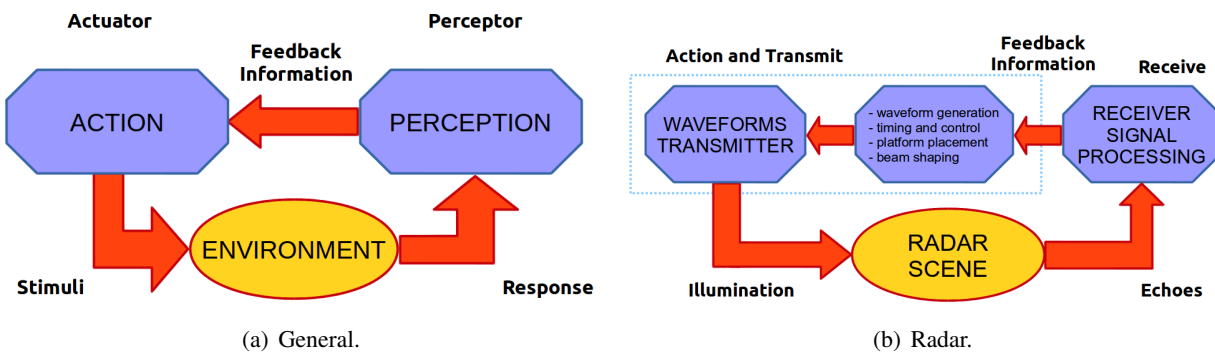
Figure 1: Schematic representation of the perception-action process.

Attention requires processing the perceptor output to extract information and to selectively concentrate on some discrete aspect of information. It can require system actions for prioritizing the allocation of available resources in accordance with their importance (for instance a detection in a give range-azimuth-Doppler bin usually involves a confirmation process which calls for a specific radar waveform optimized to the actual interference/clutter conditions and the Doppler bin under test [7], [8]). As to intelligence, among the aforementioned four functions, it is by far the most difficult to describe. While intelligence functionalities are based on the perception-action cycle, memory, and attention, it is the presence of a feedback at multiple levels that makes possible for the system intelligent decisions in face of inevitable uncertainties in the environment. As matter of fact, the presence of such a closed-loop feedback between the actuator (transmitter) and the perceptor (receiver) represents the main ingredient which makes unique the cognitive radar and clearly distinguishes it from the classic adaptive architecture. In this last case adaptivity is mainly confined at the receiver branch except for some static forms of transmit diversity [2] usually implemented in terms of mode selection (i.e. long-range versus short-range, search versus

tracking). The information sharing involved in the feedback process is complemented with the use of a memory, which in the radar case is constituted by a dynamic database. It contains knowledge sources about the operating context such as:

- geographic features of the illuminated area [9]: type of terrain, presence of clutter discretes, terrain elevation profiles (for instance gathered through Geographic Information Systems (GISs) or Digital Terrain Elevation Models (DTEMs));
- electromagnetic characteristics of the overlaid radiators: operating frequency, modulation and policy, activity profiles, location of transmitters (obtained through Radio Environment Maps (REMs) [10] which localize surrounding emissions in time, frequency, and space; and/or through spectrum sensing modules which continuously sound the environment and acquire fresh information on the external electromagnetic interference possibly used to update the content of the REMs);
- data from other sensors [11] (Synthetic Aperture Radars (SARs), infrared devices, meteorological measurements, etc.).

The overall information flow coordinates and triggers actions of the system. For example, with reference to the search process, it is exploited to devise the new transmit waveform [10], [12], to select the training data for receiver adaptation [9], [11], to censor data containing clutter discretes, to choose the most suitable detector within a battery available at the receiver. This implies a continuous adaptation of the pair perceptor-actuator ruled by the available information flow and possibly coordinated by a system manager. It is worth noting that the quoted diversity in the transmit-receive chain is actually already present in nature making the cognitive radar a bio-inspired concept. Many mammals with echolocation capabilities, in particular the bats [7, Chap. 6], in their natural behavioral phases, change the waveform in a spontaneous and systematic way, producing through tongue clicking a variety of modulated sonar signals. A nice example is the *Eptesicus Nilssonii* bat [7, Chap. 6]. While attempting to feed on prey, it changes the Pulse Repetition Time (PRT) and the waveform shape between the approach phase and the terminal phase. In fact, studying the wideband ambiguity function during the search phase, the bat is capable of resolving both in range and Doppler, then during the terminal phase, it improves the range resolution but the signal becomes quite Doppler tolerant. Interestingly, many preys also developed cognitive actions in terms of evasive behaviors [13] to counteract the bats' sonar and to confuse it with false multiple echoes (a technique which clearly resembles Electronic CounterMeasures (ECMs) to deceive a radar).

Summarizing, the block scheme of a cognitive radar is displayed in Figure 2, which, as expected, highlights the much higher hardware complexity with respect to the classic adaptive radar architecture of Figure 3.

This poses many technological challenges connected with the implementation of the new cognitive radar paradigm. Some of them can be afforded with the advent of Redundant Array of Independent Disks (RAIDs), phased array with several transmit-receive modules, Multiple-Input Multiple-Output (MIMO) hardware capabilities, multi-polarization equipments, and Application Specific Integrated Circuit (ASIC) logics, etc. Algorithmic challenges are also present in order to exploit as efficiently as possible both the feedback information and the a-priori knowledge. A multitude of algorithms should be possibly run contemporaneously, pushing for the use of parallel computing architectures and programming.

A nice and simple example of a cognitive radar tracker is shown in [14]; this is probably among the first formulations of a fore-active radar, namely a first step towards radar cognition. The measurement noise depends on the action of the transmitter. That action is controlled by a transmit waveform parameter (i.e. pulse duration and chirp rate). The optimal signal selection to sound the scene is established through a feedback between the receiver and the transmitter. By doing so, a closed-loop around the environment
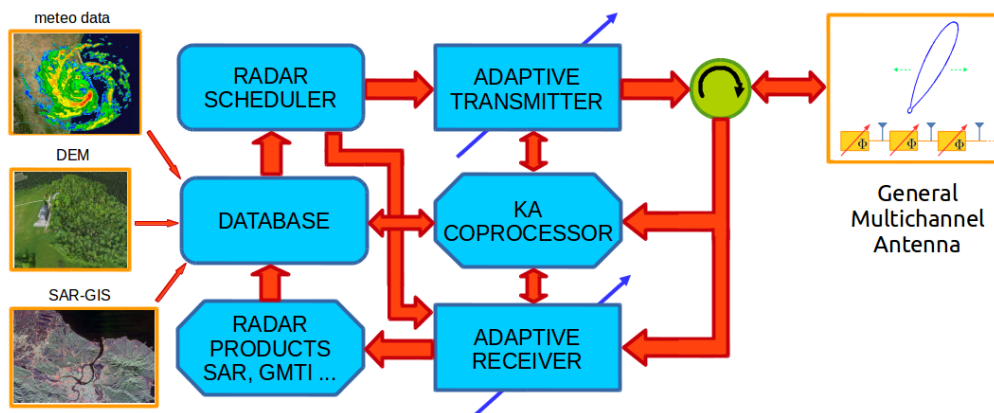
Figure 2: Block scheme of a cognitive radar.
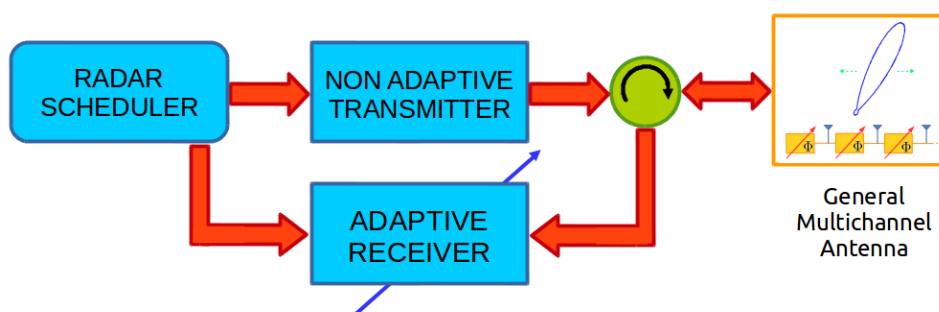
Figure 3: Classic adaptive radar architecture.

is formed, whereby it becomes possible for the transmitter to exercise indirect control on the receiver via the environment.

In the remaining part of this paper a selected list of references is first provided and then three challenging signal processing applications involving cognitive radar are presented. They can lead to a significant potential performance improvement over a classic radar system thanks to the presence of pro-activity and the interaction with a dynamic environmental database.

2. Selected Reference List on Cognitive Radar

In the following a selected reference list on cognitive radar is provided and discussed. In [15] a detailed study of a general radar system that mimics the way the visual brain observes its surrounding environment is addressed. Specifically, a cognitive radar jointly exploiting a perception-action cycle paradigm and some stored information is described. The performance gains pursued are assessed for tracking applications,

using the posterior Cramer-Rao lower bound (PCRLB) as figure of merit to dynamically adapt the transmit waveform. In [16], following the architecture in [15], a cognitive radar tracker based on the Maximum a Posteriori Penalty Function (MAP-PF) tracking methodology is described. A cognitive Pulse Repetition Frequency (PRF) adaptation is employed to enable interesting performance enhancement. In [17], resorting to a Partially Observable Markov Decision Process (POMDP) model, a new cognitive target tracker is devised. The proposed algorithm properly chooses the radar measurement times to ensure robust performance while a target becomes temporarily unobservable. By doing so a lower probability of track loss than some counterparts is achieved.

Reference [18] applies flow field theory to echolocation sensors. More precisely, it highlights that echoic flow provides key information for vehicular radar systems to create an accurate and instantaneous perception allowing automatic adjustments to be made in order to maintain safe separation.

Practical implementation issues on cognitive radar are addressed in [19]. Therein the authors demonstrate that cognitive capabilities can be readily added to modern digital radars equipped with flexible signal/data processors and arbitrary waveform synthetizers. Building upon this framework, in [20], the authors focus on a cognitive perception/action cycle for a notional fighter radar with an adaptive Active Electronic Scanning Antenna (AESA).

In [21], a cognitive radar detector is conceived exploiting previously acquired information to estimate the statistical characteristics of the operating environment. Precisely, machine learning approaches are adopted to adaptively determining the optimal detection threshold within the low sample support regime. The conducted performance analysis highlights the effectiveness of the devised algorithm to accurately estimate the threshold.

Another issue of interest which can be potentially benefit from cognition regards the coexistence of radar and communication systems. In this context, some works have been published, such as [22], where the authors introduce an approach to design shared spectrum access operations for the joint coexistence of radar and communication networks. Furthermore, in [23], an alternative approach is considered which also improves the spectral efficiency.

Last but not least, cognitive radar networks are attracting some attention in the field of environmental surveillance in the presence of non-cooperative targets [24]. The review of features, benefits, and challenges resulting in the use of such networks is also described in [25].

Notation

We adopt the notation of using boldface for vectors $\boldsymbol{a}$ (lower case), and matrices $\boldsymbol{A}$ (upper case). The conjugate transpose operator is denoted by the symbol $(\cdot)^{\dagger}$. $\boldsymbol{I}$ and $\boldsymbol{0}$ denote respectively the identity matrix and the matrix with zero entries (their size is determined from the context). $\mathbb{C}^N$ and $\mathbb{H}^N$ are respectively the sets of N-dimensional vectors of complex numbers and of $N \times N$ Hermitian matrices. The curled inequality symbol $\succeq$ (and its strict form $\succ$) is used to denote generalized matrix inequality: for any $\boldsymbol{A} \in \mathbb{H}^N$, $\boldsymbol{A} \succeq \boldsymbol{0}$ means that $\boldsymbol{A}$ is a positive semi-definite matrix ($\boldsymbol{A} \succ \boldsymbol{0}$ for positive definiteness). The letter j represents the imaginary unit (i.e. $j = \sqrt{-1}$). Finally, $\mathbb{E}\left[\cdot\right]$ denotes statistical expectation.

3. Cognitive MIMO Radar Beampattern Shaping

MIMO radar is a recently emerging paradigm enabling an enhanced performance over conventional radar in terms of target detection, identification, classification, and localization [26], [27]. Additionally, colocated MIMO radar allows a higher flexibility in the transmit beampattern shape [28] based on the ability to transmit distinct waveforms via the probing antennas.

This last feature is particularly attractive for cognitive radar systems where the transmitter dynamically selects the best transmit beampattern in response to the receiver feedbacks, accounting for both previous experience/measurements and stored information. For instance, if the receiver detects in some angles strong unwanted returns, due to both clutter discretes and non-threatening targets, the transmit beampattern can be shaped to exhibit small gain values in the mentioned directions so as to suppress the interference and to avoid overloading the processor with detections of no-tactical importance. Besides, multiple target tracking can be accomplished via multiple beams in the transmit beampattern possibly adaptively interleaved with search beams, thus enhancing the multi-functionality of the system.
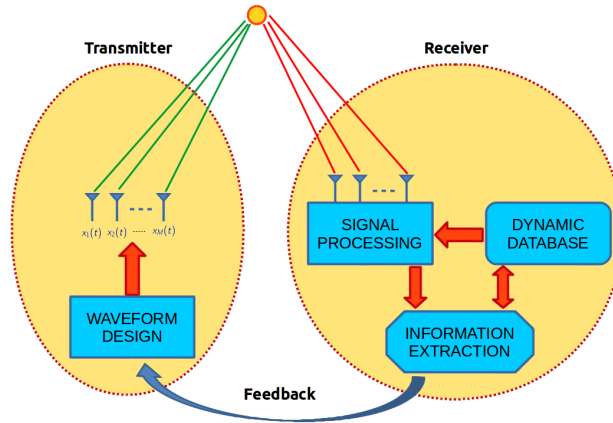
Figure 4: Cognitive MIMO radar with Transmitter/Receiver interoperability.

A colocated MIMO radar is considered where M transmit antennas are used to probe the environment. Each antenna radiates a narrow-band waveform through a non-dispersive propagation medium and $x_i(n)$, $n = 1, 2, \ldots, N$, $i = 1, \ldots, M$, are the discrete-time base-band signal transmitted by the i-th antenna, where N is the number of probing signal samples. The base-band signal arriving at the target angular location θ can be written as [28], [29]

$$y(\theta, n) = K \sum_{i=1}^{M} \exp(-j2\pi f_c \tau_i(\theta)) x_i(n), \ \ n = 1, \ldots, N, \tag{1}$$

where K is a complex parameter whose amplitude accounts for the one-way radar range equation and whose phase depends on the distance between the target and the reference antenna, f_c is the carrier frequency and $\tau_i(\theta)$ is the relative time delay between the antennas, namely the time interval accounting for the electromagnetic path between the i-th antenna and the reference one for the angular location of interest. Now, defining the steering vector $\boldsymbol{a}(\theta) \in \mathbb{C}^M$ as $\boldsymbol{a}(\theta) = [\exp(j2\pi f_c \tau_1(\theta)), \ldots, \exp(j2\pi f_c \tau_M(\theta))]^T$, the power of the transmitted signal, namely the transmit beampattern or spatial spectrum, at the location θ is proportional to (through $|K|^2$) [28]

$$P(\theta) = \frac{1}{N} \sum_{n=1}^{N} |y(\theta, n)|^2 = \boldsymbol{a}(\theta)^\dagger \boldsymbol{R} \boldsymbol{a}(\theta), \tag{2}$$

where $\boldsymbol{R} = \frac{1}{N}\sum_{n=1}^{N}\boldsymbol{x}(n)\boldsymbol{x}(n)^{\dagger} \succeq \boldsymbol{0}$, with $\boldsymbol{R} \in \mathbb{H}^M$ being the covariance matrix of the probing signal, with $\boldsymbol{x}(n) = [x_1(n), x_2(n), \ldots, x_M(n)]^T \in \mathbb{C}^M$, the MIMO radar space code at the time instant n.

In the following, θ_0 denotes the beam pointing direction and by μ_k, $k = 1, \ldots, K$, any point in the sidelobe region where possible undesired returns are foreseen. To simplify the notations, we write $\boldsymbol{a}(\theta_0), \boldsymbol{a}(\mu_1) \ldots, \boldsymbol{a}(\mu_K)$ are represented as $\boldsymbol{a}_0, \boldsymbol{a}_1 \ldots, \boldsymbol{a}_K$, respectively. Due to array non-idealities and imperfect calibration, the actual steering vector is not exactly known and the uncertainty set $\mathcal{A}_k$ associated with each steering vector is modeled through two double sided, potentially non-convex, quadratic constraints, see [30] for further technical details. Some cases of practical interest complying with the considered model are the generalized similarity with norm constraint and the conical constraint with norm constraint, [30].

Additionally, two suitable constraints on the optimization variable are forced, [30]. The former accounts for the width of the mainbeam (described through the set $\mathcal{R}_w$), whereas the latter is either a uniform (the set $\mathcal{R}_u$) or a relaxed elemental (the set $\mathcal{R}_r$) power requirement allowing to control the amount of transmitted power.

Summarizing, the robust design of the waveform covariance matrix $\boldsymbol{R}$, optimizing the worst case (over steering vector mismatches) transmit beampattern Peak Sidelobe Level (PSL), can be formulated as the following constrained max-min optimization problem

$$\underset{\boldsymbol{R} \in \mathcal{R}'}{\text{maximize}} \left[\underset{\boldsymbol{a}_k \in \mathcal{A}_k,\, k = 0, \ldots, K}{\text{minimize}} \frac{\boldsymbol{a}_0^{\dagger}\boldsymbol{R}\boldsymbol{a}_0}{\underset{k \in \{1, \ldots, K\}}{\text{maximize}} \boldsymbol{a}_k^{\dagger}\boldsymbol{R}\boldsymbol{a}_k} \right] \tag{3}$$

where $\mathcal{R}' = \mathcal{R} \cap \mathcal{R}_w$ and $\mathcal{R} \in \{\mathcal{R}_u, \mathcal{R}_r\}$.

In [30], the non-convex optimization problem (3) is studied, highlighting that an optimal robust space-time code matrix $\boldsymbol{X} = [\boldsymbol{x}(1), \boldsymbol{x}(2), \ldots, \boldsymbol{x}(N)] \in \mathbb{C}^{M \times N}$, i.e. the matrix whose n-th column, $n = 1, \ldots, N$, corresponds to the MIMO radar space code at the time instant n, can be devised with a polynomial time procedure. Specifically, problem (3) shares some hidden convexity features allowing the synthesis of the MIMO waveform covariance matrix $\boldsymbol{R} = \frac{1}{N}\boldsymbol{X}\boldsymbol{X}^{\dagger}$ maximizing the worst case PSL with a polynomial complexity. From a technical point of view (3) is equivalent to a SemiDefinite Programming (SDP) convex problem whose optimal solution $\boldsymbol{R}^{\star}$ allows the design of an optimal space-time code matrix $\boldsymbol{X}^{\star}$. Figure 5 summarizes the main steps/tricks involved in the synthesis of the optimal MIMO space-time code.

The performance of the proposed MIMO transmit beampattern design technique is analyzed focusing on a radar equipped with a Uniform Linear Array (ULA) of $M = 16$ elements (spaced half wave-length apart) and using the array boresight direction as reference angle (θ_0). Moreover, $\Omega_s = [-90, -12] \cup [12, 90]$ is chosen as sidelobe region (this selection can be driven by the memory of the system and the information flow from the receiver; for instance it might be required to focus the useful energy in a very narrow angular sector and, in this situation, the sidelobe region has to increase) and the sidelobe points μ_i $i = 1, \ldots, K$ are selected, as required in (3), uniformly dicretizing the set Ω_s, with a grid size 0.3. With reference to the uncertainty sets $\mathcal{A}_k$, $k = 0, \ldots, K$, the actual steering vector shares norm M lying within a ball centered around the nominal ULA steering direction. More details about the simulation setup are available in [30].

In Figure 6, the transmit beampattern (normalized to its value in θ_0) of the covariance matrix $\boldsymbol{R}_n$ synthesized according to (3) is plotted when no steering vector mismatches (unpredictable uncertainty
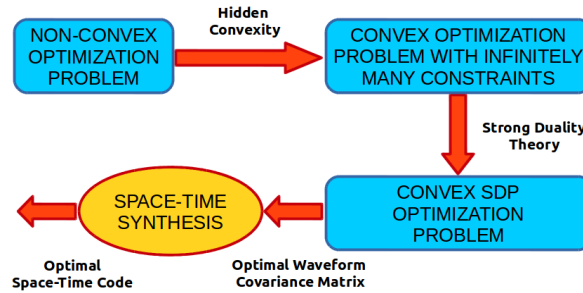
Figure 5: Block scheme of the optimization problem equivalences leading the optimal space-time code.

the system has to face with) are foreseen at the design stage. Precisely, both its normalized nominal beampattern (blue solid line) and normalized worst beampattern (blue dotted line) are reported. For comparison purposes, it is also plotted $P(\theta)$ (normalized to its value in θ_0) of the covariance $\bar{R}_n$ obtained resorting to the algorithm proposed in [26] (red dashed line for the normalized nominal beampattern and red dashed-dotted line for the normalized worst beampattern).

The results show that R_n shares a PSL value higher than $\bar{R}_n$ of about 5 dB in the matched operative conditions, highlighting the effectiveness of the new technique. Nevertheless, steering mismatches severely impair the performance of both R_n and $\bar{R}_n$, further confirming the interest toward a robust design approach. Interestingly, also the worst beampattern of R_n outperforms $\bar{R}_n$ in terms of PSL.
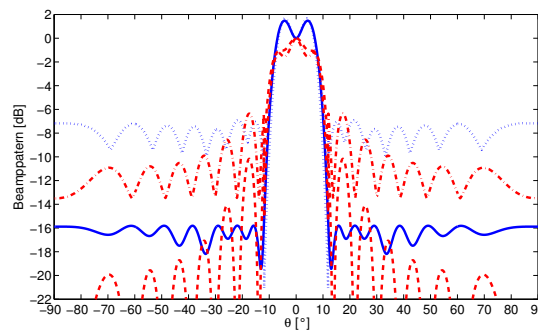
Figure 6: Normalized $P(\theta)$ versus θ: nominal beampattern of R_n blue solid line, worst beampattern of R_n blue dotted line, nominal beampattern of $\bar{R}_n$ red dashed line, and worst beampattern of $\bar{R}_n$ red dashed-dotted line. A uniform elemental power constraint is enforced.

In Figure 7, the normalized $P(\theta)$ of the optimal covariance matrix R_r devised according to (3) is depicted, when the array manifold uncertainties are properly modeled at the design stage. Both the normalized nominal and the worst beampattern are illustrated, (blue solid line for the former and blue

dotted line for the latter). For comparison purposes, the normalized radiation pattern of the covariance $\bar{R}_r$ obtained through the algorithm in [29] is also shown, where the norm constraint can not be enforced. Precisely, in Figure 7, the red dashed curve refers to the normalized nominal beampattern of $\bar{R}_r$, the red dashed-dotted line accounts for the normalized worst beampattern of $\bar{R}_r$, and the green ●-marked curve relates to the normalized worst beampattern of R_n. The plots reveal the ability of the described algorithm to devise a covariance ensuring an enhanced worst case performance level, in terms of PSL, with respect to the considered counterparts. It thus represents a very flexible and robust technique guided by cognition in the process of focusing the beams, ruling the sidelobe region, putting angular nulls. In other words, the correct stimulation for probing the specific scene it adopts.
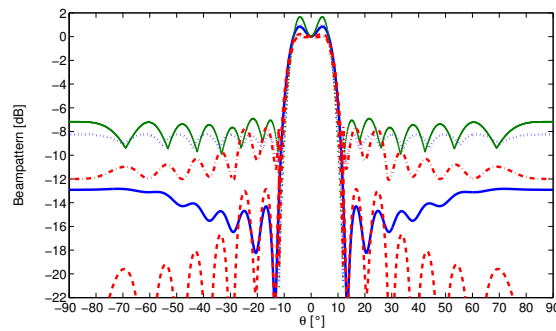
Figure 7: Normalized $P(\theta)$ versus θ: nominal beampattern of R_r blue solid line, worst beampattern of R_r blue dotted line, nominal beampattern of $\bar{R}_r$ red dashed line, worst beampattern of $\bar{R}_r$ red dashed-dotted line, and worst beampattern of R_n green ●-marked curve.

4.   Cognitive CFAR Processing Techniques

To mitigate the deleterious effects of clutter and jammer, modern radars have employed adaptive processing techniques such as Constant False Alarm Rate (CFAR) detectors, adaptive arrays, and Space Time Adaptive Processing (STAP) [31]. Typical adaptive algorithms estimate the disturbance covariance matrix of the data under test (primary data) using training (secondary) data collected from range cells in close proximity to the one under test with the assumption that primary and secondary data share the same spectral properties. However, this assumption is not always verified (training data are often contaminated by power and spectral variations over range, clutter discretes, and other outliers) and poor training data selection can produce significant performance degradation in terms of high false alarm rate and/or low detection probability [32].

To overcome this drawback the cognitive paradigm can be pursued assuming the presence of a look-ahead processor [2] which projects a few seconds into the future to determine where the radar will be and what it will be doing. This information permits to access the memory information whose processing raises the attention on some specific task (for instance the presence of a range cell which contains a strong clutter discrete) and pushes for a subsequent action (training data selection, outlier rejection, etc.). Possible sources of information for this context are DTEMs, previous radar experiences, GISs, roadway

maps (to highlight sectors of surveillance where moving cars or vehicles might be present), background of air/surface traffic, meteorological data, some electromagnetic reflectivity and spectral clutter models, system calibration information, which can be dynamically updated.

Let us focus on the problem of establishing whether or not a single-bin post-Doppler STAP [9], [31] contains a prospective target. Denote by $r \in \mathbb{C}^N$ the vector of the primary data, the detection problem at hand can be formulated as the following binary hypothesis test

$$\begin{cases} H_0: & r = c, \\ H_1: & r = \alpha s + c, \end{cases} \tag{4}$$

where $s \in \mathbb{C}^N$ is the filtered target space-time steering vector at the considered Doppler bin, $\alpha \in \mathbb{C}$ is an unknown deterministic parameter accounting for both target reflectivity and channel propagation effects, and c accounts for the disturbance in the range cell under test.

In many practical applications, the covariance matrix of c is unknown and a set of secondary data r_i, $i = 1, \ldots, H$, namely Doppler-filtered vectors from range cells surrounding the one being tested and referring to the same Doppler bin of r are used to estimate the disturbance covariance. As already pointed out, not all the secondary data are representative of the probed cell and to overcome this shortcoming a cognitive architecture, like that depicted in Figure 8, comes in handy.
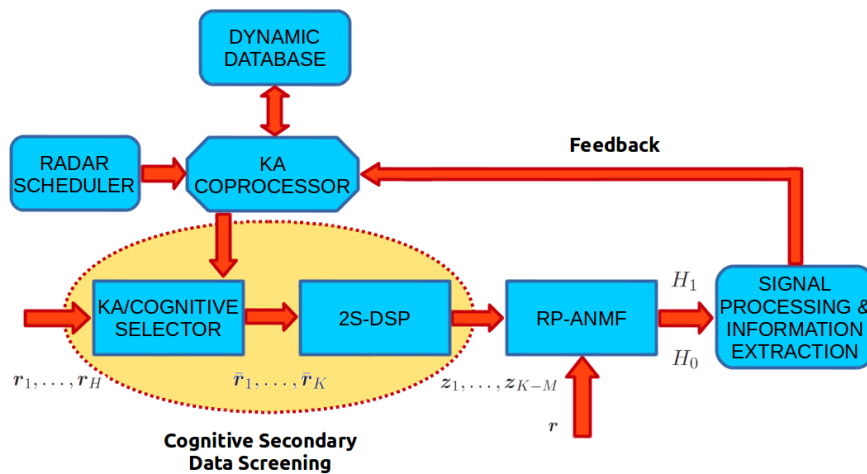
Figure 8: Block diagram of the KA-RP-ANMF detector.

The first block implements a Knowledge-Aided (KA)/cognitive data selection resorting to the algorithm devised in [33] which utilizes terrain data from the U.S. Geological Survey (USGS) to aid the data selection process. The second block is the Two-Step Data Selection Procedure (2S-DSP), a data-adaptive selection algorithm devised in [34], which attempts to adaptively remove dynamic outliers and other residual nonhomogeneities from the training set. Finally, the third block is the Recursive Persymmetric Adaptive Normalized Matched Filter (RP-ANMF) [35], which performs the final decision concerning the target presence processing the primary and the secondary data which pass the cognitive screening process.

KA/Cognitive Data Selector: The basic assumption of the KA/cognitive selection algorithm is that the dominant clutter competing with targets in the test cell is due to the patch of Earth (later referred to as the test clutter cell) within the same test ring, and corresponding to the target Doppler. As a consequence the data selector chooses secondary range-Doppler cells that have the "same" terrain as the test clutter cell. To this end it exploits National Land Cover Data (NLCD) [36] to classify the ground environment illuminated by the radar. The NLCD data were obtained from the USGS in a grid cell format with a
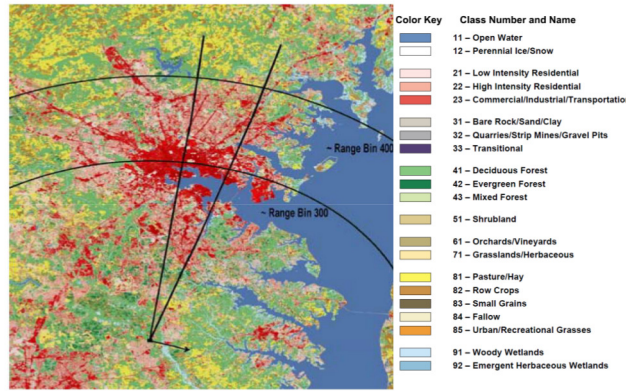
Figure 9: Example of terrain map and its legend.

spatial resolution of 30 meters. The terrain is hierarchically grouped by 9 major classifications such as urban areas, barren land, water, etc., and subgrouped into 21 minor classifications such as high intensity residential urban areas, low intensity residential urban areas, etc, as shown in Figure 9.

Through the NLCD interrogation, some suitable quantitative features/attributes can be assigned to each range-Doppler cell, depending on the type of terrain composing the analyzed cell. Hence, the features of each potential secondary data cells are compared with those of the test clutter cell computing the squared norm difference. Cells with lower grades are assumed to better match the test clutter cell. The grades are then sorted in decreasing order and the last K cells are chosen as secondary data, see [9] for further details.

2S-DSP Data Selection Procedure: This is a data-driven selector which chooses the most-homogeneous training vectors according to a statistical measure of proximity [9], [34].

RP-ANMF Detector: It has been devised in [35] and, under its design condition, it is capable of ensuring the CFAR property with respect to both the clutter powers as well as the clutter covariance structure [35]. Specifically, the RP-ANMF is defined as the following decision rule

$$\frac{|\boldsymbol{s}^{\dagger}\widehat{\boldsymbol{\Sigma}}^{-1}\boldsymbol{r}|^{2}}{(\boldsymbol{r}^{\dagger}\widehat{\boldsymbol{\Sigma}}^{-1}\boldsymbol{r})\,(\boldsymbol{s}^{\dagger}\widehat{\boldsymbol{\Sigma}}^{-1}\boldsymbol{s})} \underset{H_0}{\overset{H_1}{\gtrless}} T \tag{5}$$

where T is the detection threshold, and $\widehat{\Sigma}$ is the recursive persymmetric covariance structure estimator [35].

The performance of the illustrated system is analyzed in comparison with three adaptive processors available in the open literature: 1) the Modified Sample Matrix Inversion (MSMI) detector which does not exploit any selection algorithms; 2) the Modified Sample Matrix Inversion (MSMI) detector with the KA data selector; 3) the 2S-DSP-RP-ANMF namely the KA-RP-ANMF without the KA stage. See [9] for additional details.

All the analysis is conducted on measured airborne radar data obtained from the AFRL Sensors Directorate's MCARM program. The datasets consist of multi-channel clutter data collected by an airborne platform with a side looking radar sharing a range resolution of approximately 120 meters. Each CPI consisted of 128 pulses and the clutter was typically unambiguous in Doppler. The digital terrain map corresponding to the considered dataset is illustrated in Figure 9 where different colors are used to denote different attributes of the scene. Further information about experimental dataset can be found in [9].

The first results concern the CFAR behavior of the four analyzed systems. The threshold of the receivers are set in order to ensure a Probability of False Alarm (P_{fa}) equal to 10^{-2} in the presence of homogeneous Gaussian white noise. Then the number of threshold crossings of the decision statistics in the presence of the measured radar data is evaluated. In Figures 10(a), 10(b), 10(c), 10(d) the decision statistics are plotted versus the cell number for $K = 45$, $N = 22$, $M = 5$, angle bin 65 (corresponding to boresight), and Doppler bin 40. The plots clearly show that the advanced system presents a number of false alarms smaller than the number exhibited by the other analyzed processors. More precisely the new system shows zero false alarms out of 100 trials ($0/100$), which agrees with the nominal P_{fa} value. The KA-MSMI, the plain MSMI, and the 2S-DSP-RP-ANMF show respectively $3/100$, $38/100$, and $8/100$ false alarms.
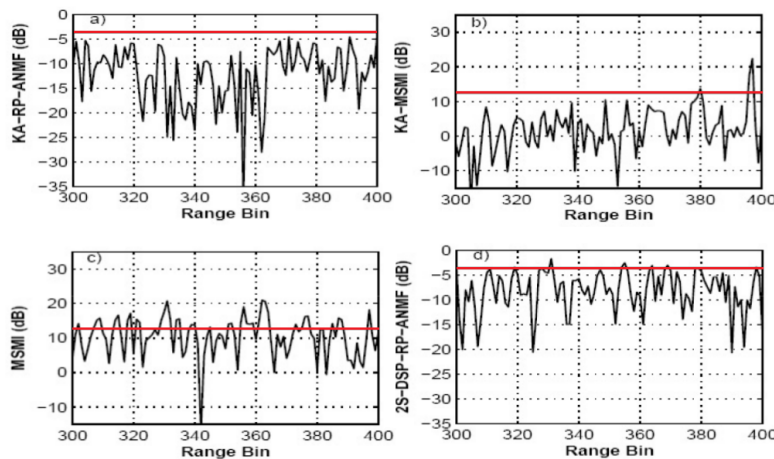
Figure 10: Decision statistic versus the cell number for $K = 49$, $N = 22$, $M = 5$, angle bin 65, and Doppler bin 40. a) KA-RP-ANMF, b) KA-MSMI, c) MSMI, d) 2S-DSP-RP-ANMF. Straight line: detection threshold for $P_{fa} = 10^{-2}$.

Finally, some results concerning the capabilities of the analyzed algorithms to detect a target are provided. To this end a synthetic target is injected in a given range cell and the detection capabilities of

the algorithms are studied. The Signal-to-Clutter Power Ratio (SCR) is defined as SCR $= \frac{|\alpha|^2}{\overline{\sigma^2}}$, where $\overline{\sigma^2}$ is the average clutter power estimated from the measured dataset.

In Figures 11(a), 11(b), 11(c), 11(d) a target with SCR$= 0$ dB is injected in the range bin 312, assuming $K = 49$, $N = 22$, $M = 5$, angle bin 65, and Doppler bin 40. The plots clearly indicate that all the analyzed detectors are capable of detecting the target. A similar behavior is obtained for SCR$= -5$ dB. This is a clear evidence of the benefits that cognition could provide to radar detection.
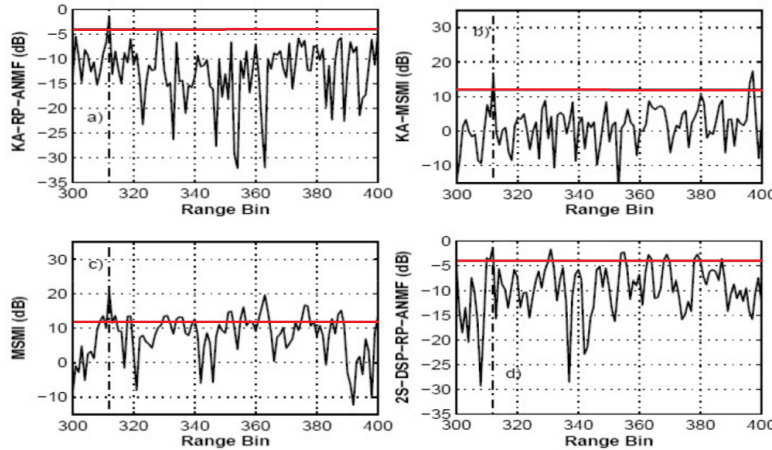
Figure 11: Decision statistic versus the cell number for $K = 49$, $N = 22$, $M = 5$, angle bin 65, Doppler bin 40, and target with SCR$= 0$ dB (injected at the range bin 312, angle bin 65, Doppler bin 40). a) KA-RP-ANMF, b) KA-MSMI, c) MSMI, d) 2S-DSP-RP-ANMF. Straight line: detection threshold for $P_{fa} = 10^{-2}$.

5.   Exploiting Multiple A-Priori Spectral Models for Detection

The idea pursued in this section is to gain receiver adaptivity through the use of multiple a-priori covariance models selected and updated according to a cognitive perspective. Exploiting the feedback from the perceptor, information from GISs, DTEMs, meteorological data, previous experiences, and environmental responses are used to formulate some spectral models for the Power Spectral Density (PSD) of the interference, see Figure 12, which can be suitably "combined" to get an estimate of the actual disturbance covariance matrix [37], [38]. As an example, from the look-ahead processor, it is possible to have a rough view of the scene which will be sounded by the radar some instants after the present one. Based on this, the most suitable models to represent its spectral properties can be selected from memory (a dynamic library) and merged together to construct a covariance estimator.

According to this guideline and resorting to the Maximum Likelihood (ML) principle, some constrained estimates of the unknown parameters can be conceived and exploited to devise two Generalized Likelihood Ratio Test (GLRT) based detectors for the radar problem [39].

Let us consider a monostatic radar that transmits a coherent train of N pulses and denote by $\boldsymbol{r} \in \mathbb{C}^N$ the N-dimensional vector of the samples obtained after base-band conversion, filtering, and sampling at
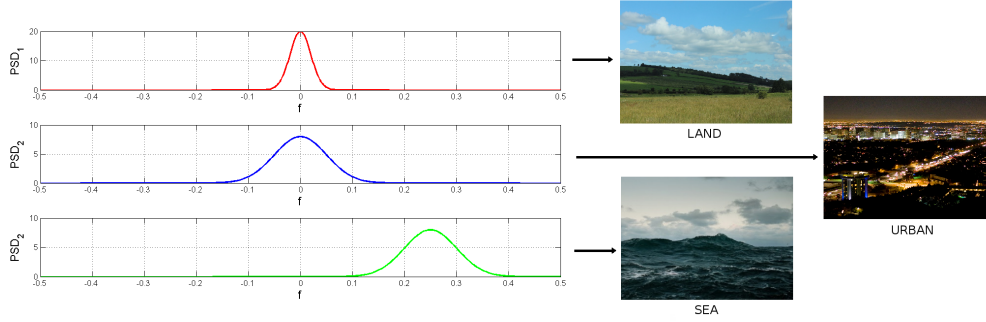
Figure 12: PSD examples related to different scenarios.

the range of interest the incoming waveform (primary data). The availability of secondary data $\boldsymbol{r}_i \in \mathbb{C}^N$, $i = 1, \cdots, K, \ (K \geq 0)$, is assumed which do not contain useful target signal and exhibit the same covariance matrix[1] as the primary data. The following binary hypothesis testing problem is considered

$$\begin{cases} H_0 : \ \boldsymbol{r} = \boldsymbol{n}, \ \boldsymbol{r}_i = \boldsymbol{n}_i, \ i = 1, \cdots, K \\ H_1 : \ \boldsymbol{r} = \boldsymbol{n} + \alpha \boldsymbol{p}, \ \boldsymbol{r}_i = \boldsymbol{n}_i, \ i = 1, \cdots, K \end{cases} \tag{6}$$

where $\boldsymbol{p} \in \mathbb{C}^N$ denotes the unitary norm steering vector of the target and $\alpha \in \mathbb{C}$ is an unknown parameter accounting for both target reflectivity and channel propagation effects. As to the interference plus noise random vectors, $\boldsymbol{n}$ and $\boldsymbol{n}_i$'s, $i = 1, \cdots, K$, are independent, complex, zero-mean, circular symmetric Gaussian vectors sharing the same covariance matrix $\boldsymbol{M} \succ \boldsymbol{0}$, namely $\mathbb{E}[\boldsymbol{n}\boldsymbol{n}^\dagger] = \mathbb{E}[\boldsymbol{n}_i \boldsymbol{n}_i^\dagger] = \boldsymbol{M}$, $i = 1, \ldots, K$, and denote the inverse covariance matrix $\boldsymbol{M}^{-1}$ with $\boldsymbol{X}$.

The idea is to exploit the memory about the interfering environment so as to suitably describe, and hence constrain, the interference plus noise covariance matrix. By doing so, the sample support requirement is reduced while keeping good detection performance [39]. In particular, it is assumed:

- the availability of multiple a-priori models for the interference PSD (see Figure 12) [39]. Each of them corresponds to a model for the inverse interference covariance matrix $\boldsymbol{X}$; these inverse covariance models, $\boldsymbol{X}_i$, $i = 0, \ldots, H$, are assumed positive definite, i.e. $\boldsymbol{X}_i \succ \boldsymbol{0}$, $i = 0, \ldots, H$;
- the availability of a lower bound σ^2 on the PSD level of the white disturbance term σ_0^2, i.e. $\sigma_0^2 \geq \sigma^2$.

Otherwise stated, it is supposed that $\boldsymbol{X}$ belongs to the uncertainty set

$$\mathcal{A} = \left\{ \boldsymbol{X}' \succ \boldsymbol{0} : \ \boldsymbol{X}' = \sum_{i=0}^{H} t_i \boldsymbol{X}_i, \ \boldsymbol{X}' \preceq \frac{\boldsymbol{I}}{\sigma^2}, \ t_i \in \mathbb{R}, i = 0, \ldots, H \right\}. \tag{7}$$

A possible strategy to estimate the unknown parameters α and $\boldsymbol{X}$ accounting for the covariance structure (7), is to resort to the constrained ML approach. Specifically, some approximate versions of the GLRT

---

[1]Notice that, from a practical point of view, a data selection scheme, such as that in [40] or [41], can be employed to pre-process the available training data so as to excise possible outliers.

[39] can be conceived assuming that the unknown parameters comply with the conditions $\boldsymbol{X} \in \mathcal{A}$. In particular, two detectors are here discussed:

1) GLRT-1: Involves the solution of MAXDET convex optimization problems [39], which can be efficiently handled using interior point methods with a polynomial worst case computational complexity.

2) GLRT-2: Exploits sub-optimum estimates of the unknown parameters [39].

Their performance is analyzed in terms of detection probability P_d also in comparison with the optimum detector, which assumes the perfect knowledge of the disturbance covariance matrix, Kelly's GLRT, and AMF. The available multiple a-priori models for the interference covariance matrix are assumed Gaussian shaped [42], namely

$$\boldsymbol{M}_i(h,k) = \rho_i^{(h-k)^2} \exp[j2\pi(h-k)f_i] + 10^{-2}\delta_{h,k} , \, i = 1, \ldots, H$$

where $\delta_{h,k}$ denotes the Kronecker delta function, ρ_i is the one-lag correlation coefficient and f_i represents the normalized Doppler frequency. Moreover, $\boldsymbol{M}_0$ has been set equal to $\boldsymbol{I}$ to account for the receiver noise floor. As to the actual covariance matrix, an interference sharing a bimodal PSD is considered accounting for the presence of ground and sea clutters in addition to white noise. Precisely, assuming an exponentially-shaped PSD for both the interfering sources, we have

$$\boldsymbol{M}(h,k) = \text{CNR}_s \, \rho_s^{|h-k|} \exp[j2\pi(h-k)f_s] + \text{CNR}_g \, \rho_g^{|h-k|} \exp[j2\pi(h-k)f_g] + \delta_{h,k} , \qquad (8)$$

where CNR_s and CNR_g denote, respectively, the Clutter-to-Noise-Ratio (CNR) for the sea and the ground clutter; ρ_s and ρ_g are, respectively, the one-lag correlation coefficients for the sea and the ground clutter; f_s and f_g, are, respectively, the normalized Doppler frequency for the sea and the ground clutter. As to the Doppler steering vector, $\boldsymbol{p} = \frac{1}{\sqrt{N}}[1, e^{j2\pi f_d}, \ldots, e^{j2\pi f_d(N-1)}]^T$, where f_d is the normalized target Doppler frequency. In all the simulations, the parameters specified in Table I are considered; additionally, the Doppler frequencies of the a-priori models, $\boldsymbol{X}_i$, $i = 1, \ldots, H$, are uniformly distributed over the frequency range $\left[-\frac{1}{2}, \frac{1}{2}\right[$, i.e. $f_i = -0.5 + \left(\frac{i-1}{H}\right)$, $i = 1, \ldots, H$.

Parameter	N	f_d	f_g	f_s	ρ_i	ρ_g	ρ_s	σ^2 [dB]	CNR_g [dB]	CNR_s [dB]
Value	10	0.20	0.05	0.285	0.90	0.93	0.85	-10	30	20

TABLE I: Parameters used at analysis stage.

The performances are given in terms of P_d versus the Signal-to-Interference plus Noise Ratio (SINR), defined as $\text{SINR} = |\alpha|^2 \boldsymbol{p}^\dagger \boldsymbol{M}^{-1}\boldsymbol{p}$, setting $P_{fa} = 10^{-2}$.

Figures 13(a), 13(b) show, respectively, the results obtained considering $H = 14$ and $H = 20$. The resulting curves highlight that with such a limited amount of secondary data ($K = 10$), the AMF and the Kelly's GLRT exhibit unsatisfactory performances, and the multiple-model based receivers are a viable mean to compensate for the loss experienced by the conventional adaptive structures. Furthermore, increasing the adopted model number, the new detectors significantly outperform the conventional ones. As expected, GLRT-1 outperforms GLRT-2, which, on the other hand, requires a much lower computational complexity. Figure 13(c) show the results obtained considering $H = 20$ and $K = 20$. The resulting curves highlight that the performances of the AMF and Kelly's GLRT significantly improve with respect to the case $K = 10$, but they are still outperformed by the multiple-model based detectors.

(a)

(b)

(c)
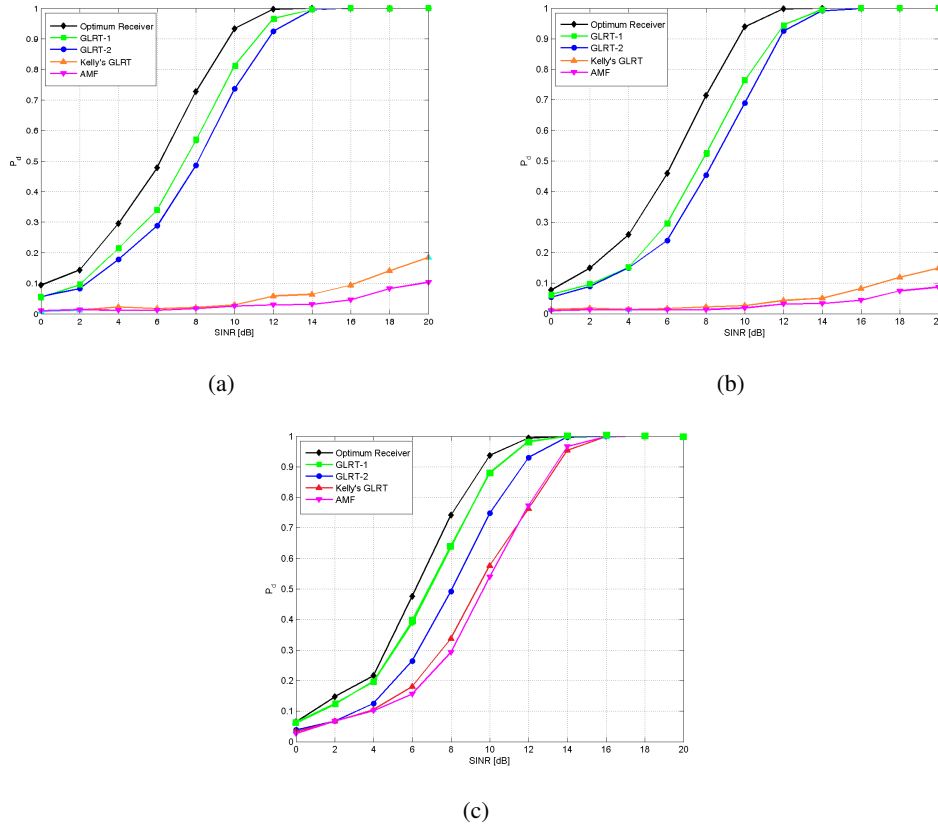
Figure 13: P_d versus SINR assuming $P_{fa} = 10^{-2}$ for the parameters specified in Table I. a) $K = 10$, $H = 14$, b) $K = 10$, $H = 20$, c) $K = 20$, $H = 20$.

6.   Conclusions: Lessons Learned

Cognitive radar concept has been explored explaining the inspiring principles and illustrating the basic system architecture also in comparison with a classic adaptive radar. Some distinctive features have been highlighted:

Adaptivity. It must learn as information changes, and as goals and requirements evolve. At the same time it must tolerate unpredictability.

Mindful. It must "remember" previous experiences and interactions with the environment returning information that is suitable for the specific application at the right time.

Contextual. It must understand, identify, and extract contextual elements. It may draw on multiple sources of information, including environmental database, as well as sensory inputs (received radar).

Intelligent. It must possess a decision-making mechanism, heavily exploiting the closed-loop feedback between the transmit and receive chain, which determines some system actions.

In the second part of the paper a selected list of references has been provided and three challenging radar signal processing applications which could possibly benefit from cognition have been presented together with the potential performance gain over the classic architecture.

Some important lessons learned from cognitive radar can be summarized as follows [1], [4]: (i) when an application of interest closely follows human cognition in conceptual terms, we could look into the perception-action cycle for the structural design of a cognitive dynamic system to satisfy the practical requirements of that particular application. (ii) When, on the other hand, the application of interest lends itself to the use of cognition but does not closely follow human cognition in conceptual terms, we may look to the human brain for inspiration with the objective of identifying those learning tools that are relevant to that context.

References

[1] S. Haykin, *Cognitive Dynamic Systems: Perception-Action Cycle, Radar and Radio*, Cambridge University Press, 2012.

[2] J. R. Guerci, *Cognitive Radar: The Knowledge-Aided Fully Adaptive Approach*, Artech House, 2010.

[3] S. Haykin, "Cognitive Radar: a Way of the Future," *IEEE Signal Processing Magazine*, vol. 23, no. 1, pp. 30–40, January 2006.

[4] S. Haykin, "Cognitive Dynamic Systems: Radar, Control, and Radio [Point of View]," *Proceedings of the IEEE*, vol. 100, no. 7, pp. 2095–2103, July 2012.

[5] J. Ender and S. Bruggenwirth, "Cognitive Radar - Enabling Techniques for Next Generation Radar Systems," in *International Radar Symposium (IRS)*, June 2015.

[6] M. Wicks, "Spectrum Crowding and Cognitive Radar," in *International Workshop on Cognitive Information Processing*, June 2010.

[7] F. Gini, A. De Maio, and L. K. Patton, *Waveform Design and Diversity for Advanced Radar Systems (IET Radar, Sonar and Navigation)*, IET Series 22, Institution of Engineering and Technology, 2012.

[8] A. De Maio, S. De Nicola, Y. Huang, S. Zhang, and A. Farina, "Code Design to Optimize Radar Detection Performance Under Accuracy and Similarity Constraints," *IEEE Transactions on Signal Processing*, vol. 56, no. 11, pp. 5618–5629, November 2008.

[9] C. T. Capraro, G. T. Capraro, A. De Maio, A. Farina, and M. Wicks, "Demonstration of Knowledge Aided Space-Time Adaptive Processing Using Measured Airborne Data," *IEE Proceedings Radar, Sonar and Navigation*, vol. 153, no. 6, pp. 487–494, December 2006.

[10] A. Aubry, A. De Maio, M. Piezzo, and A. Farina, "Radar Waveform Design in a Spectrally Crowded Environment via Nonconvex Quadratic Optimization," *IEEE Transactions on Aerospace and Electronic Systems*, vol. 50, no. 2, pp. 1138–1152, April 2014.

[11] F. Gini and M. Rangaswamy, *Knowledge Based Radar Detection, Tracking and Classification*, vol. 52, John Wiley & Sons, 2008.

[12] A. Aubry, A. De Maio, A. Farina, and M. Wicks, "Knowledge-Aided (Potentially Cognitive) Transmit Signal and Receive Filter Design in Signal-Dependent Clutter," *IEEE Transactions on Aerospace and Electronic Systems*, vol. 49, no. 1, pp. 93–117, January 2013.

[13] L. A. Miller and A. Surlykkej, "How Some Insects Detect and Avoid Being Eaten by Bats: Tactics and Countertactics of Prey and Predator," *BioScience*, vol. 51, no. 7, July 2001.

[14] D. J. Kershaw and R. J. Evans, "Optimal Waveform Selection for Tracking Systems," *IEEE Transactions on Information Theory*, vol. 40, no. 5, pp. 1536–1550, September 1994.

[15] S. Haykin, Y. Xue, and P. Setoodeh, "Cognitive Radar: Step Toward Bridging the Gap Between Neuroscience and Engineering," *Proceedings of the IEEE*, vol. 100, no. 11, pp. 3102–3130, November 2012.

[16] K. L. Bell, J. T. Johnson, G. E. Smith, C. J. Baker, and M. Rangaswamy, "Cognitive Radar for Target Tracking using a Software Defined Radar System," in *2015 IEEE Radar Conference (RadarCon)*, May 2015, pp. 1394–1399.

[17] A. Charlish and F. Hoffmann, "Anticipation in Cognitive Radar using Stochastic Control," in *2015 IEEE Radar Conference (RadarCon)*, May 2015, pp. 1692–1697.

[18] C. J. Baker, G. E. Smith, A. Balleri, M. Holderied, and H. D. Griffiths, "Sensing, Cognition, and Engineering Application [Further Thoughts]," *Proceedings of the IEEE*, vol. 102, no. 4, pp. 459–459, April 2014.

[19] D. M. Zasada, J. J. Santapietro, and L. D. Tromp, "Implementation of a Cognitive Radar Perception/Action Cycle," in *2014 IEEE Radar Conference*, May 2014, pp. 544–547.

[20] D. M. Zasada, M. C. Arabadjis, and L. D. Tromp, "A Cognitive Perception/Action Cycle for a Notional Fighter Radar," in *2015 IEEE Radar Conference (RadarCon)*, May 2015, pp. 1739–1743.

[21] J. Metcalf, S. D. Blunt, and B. Himed, "A Machine Learning Approach to Cognitive Radar Detection," in *2015 IEEE Radar Conference (RadarCon)*, May 2015, pp. 1405–1411.

[22] J. R. Guerci, R. M. Guerci, A. Lackpour, and D. Moskowitz, "Joint Design and Operation of Shared Spectrum Access for Radar and Communications," in *2015 IEEE Radar Conference (RadarCon)*, May 2015, pp. 761–766.

[23] Kuan-Wen Huang, M. Bica, U. Mitra, and V. Koivunen, "Radar Waveform Design in Spectrum Sharing Environment: Coexistence and Cognition," in *2015 IEEE Radar Conference (RadarCon)*, May 2015, pp. 1698–1703.

[24] S. Haykin, "Cognitive Radar Networks," in *1st IEEE International Workshop onComputational Advances in Multi-Sensor Adaptive Processing, 2005*, December 2005, pp. 1–3.

[25] H. Griffiths and C. J. Baker, "Towards the Intelligent Adaptive Radar Network," in *2013 IEEE Radar Conference (RADAR)*, April 2013, pp. 1–5.

[26] J. Li and P. Stoica, "MIMO Radar with Colocated Antennas," *IEEE Signal Processing Magazine*, vol. 24, no. 5, pp. 106–114, September 2007.

[27] A. M. Haimovich, R. S. Blum, and L. J. Cimini, "MIMO Radar with Widely Separated Antennas," *IEEE Signal Processing Magazine*, vol. 25, no. 1, pp. 116–129, January 2008.

[28] P. Stoica, J. Li, and Yao Xie, "On Probing Signal Design For MIMO Radar," *IEEE Transactions on Signal Processing*, vol. 55, no. 8, pp. 4151–4161, August 2007.

[29] N. Shariati, D. Zachariah, and M. Bengtsson, "Minimum Sidelobe Beampattern Design for MIMO Radar Systems: A Robust Approach," in *2014 IEEE International Conference on Acoustics, Speech and Signal Processing (ICASSP)*, May 2014, pp. 5312–5316.

[30] A. Aubry, A. De Maio, and Y. Huang, "PSL-based Beampattern Design for MIMO Radar Systems," in *2015 IEEE Radar Conference (RadarCon)*, May 2015, pp. 231–236.

[31] J. Ward, "Space-Time Adaptive Processing for Airborne Radar," Technical Report 1015, Massachussets Institute of Technology Lincoln Laboratories, December 1994.

[32] W. L. Melvin, "Space-Time Adaptive Radar Performance in Heterogeneous Clutter," *IEEE Transactions on Aerospace and Electronic Systems*, vol. 36, no. 2, pp. 621–633, Aprile 2000.

[33] C. T. Capraro, G. T. Capraro, D. D. Weiner, and M. Wicks, "Knowledge Based Map Space Time Adaptive Processing (KBMapSTAP)," in *Proceedings of the 2001 International Conference on Imaging Science, Systems, and Technology*, June 2001, pp. 533–538.

[34] E. Conte, A. De Maio, A. Farina, and G. Foglia, "Design and Analysis of a Knowledge-Based Radar Detector for Doppler Processing," *IEEE Transactions on Aerospace and Electronic Systems*, vol. 42, no. 3, pp. 1058–1079, July 2006.

[35] E. Conte and A. De Maio, "Mitigation Techniques for Non-Gaussian Sea Clutter," *IEEE Journal of Oceanic Engineering*, vol. 29, no. 2, pp. 284–302, April 2004.

[36] National Land Cover Data (NLCD), "http://landcover.usgs.gov/prodescription.asp," .

[37] M. Steiner and K. Gerlach, "Fast Converging Adaptive Processors or a Structured Covariance Matrix," *IEEE Transactions on Aerospace and Electronic Systems*, vol. 36, no. 4, pp. 1115–1126, October 2000.

[38] A. Aubry, A. De Maio, and V. Carotenuto, "Optimality Claims for the FML Covariance Estimator with respect to two Matrix Norms," *IEEE Transactions on Aerospace and Electronic Systems*, vol. 49, no. 3, pp. 2055–2057, July 2013.

[39] A. Aubry, V. Carotenuto, A. De Maio, and G. Foglia, "Exploiting Multiple a-priori Spectral Models for Adaptive Radar Detection," *IET Radar, Sonar Navigation*, vol. 8, no. 7, pp. 695–707, August 2014.

[40] A. Aubry, A.D. Maio, L. Pallotta, and A. Farina, "Covariance Matrix Estimation via Geometric Barycenters and its Application to Radar Training Data Selection," *IET Radar, Sonar Navigation*, vol. 7, no. 6, pp. 600–614, July 2013.

[41] P. Chen, W. L. Melvin, and M. Wicks, "Screening Among Multivariate Normal Data," *Journal of Multivariate Analysis*, vol. 69, no. 1, pp. 10–29, April 1999.

[42] A. Farina, F. Gini, M. V. Greco, and P. H. Y. Lee, "Improvement Factor for Real Sea-Clutter Doppler Frequency Spectra," *IEE Proceedings Radar, Sonar and Navigation*, vol. 143, no. 5, pp. 341–344, October 1996.